Endofullerenes: A New Family of Carbon Clusters, Ed. T. Akasak & S. Nagase,
Kluwer Academic, Dordrecht, Netherlands, 2001

Chapter 14

ENDOHEDRAL METALLOFULLERENE IN GAS PHASE

Shigeo Maruyama
Department of Mechanical Engineering, The University of Tokyo, 7-3-1 Hongo, Bunkyo-ku, Tokyo 113-8656, Japan

Abstract, Mass-spectroscopic experiments related to the endohedral metallofullerene are reviewed. Generation techniques of gas phase clusters, FT-ICR mass spectroscopy experiments, and ion mobility experiments are overviewed. Based on those experimental results, the formation mechanism of endohedral metallofullerene is discussed with classical molecular dynamics simulation results. Finally, exotic predictions from the mass spectroscopic experiments such as new types of heterofullerene, Met-Cars, small cage endohedral metallofullerene and more are discussed.

Key words, Endohedral metallofullerene, Gas phase, Mass spectrometry, Molecular dynamics

1. INTRODUCTION

At the time of the discovery of C_{60} by Kroto et al. [1] in 1985, the endohedral metallofullerene was already suggested in the mass-spectroscopic experiment [2]. Actually, the shrink-wrapping photo-dissociation [3] with loss of C_2 units down to the certain carbon size depending on the metal species [4] was one of the important evidence of the hypothesis of spherical cage structure of C_{60} [5]. The information obtained by the mass-spectroscopic experiments at the time was mass abundance distribution, chemical reactivity [2,4], laser photodissociation pattern [4], collisional dissociation pattern, and UPS (ultraviolet photoelectron) spectroscopy [6]. Later, ion chromatography experiments used for carbon

clusters by Bowers et al. [7-9] and Jarrold et al. [10-12] gave another measure of geometric structure of clusters. However, after the discovery of the macroscopic generation technique [13] and isolation technique [14,15], the relative importance of the mass-spectroscopic experiments declined compared to the really direct X-ray diffraction demonstrations [16]. Exactly the same situation was in the studies of empty fullerenes. The mass spectroscopic experiments had been most important when the idea of exotic structure of clusters were examined [1], but all other macroscopic experiments could give much concrete results after the discovery of the macroscopic generation and isolation technique [17,18].

However, the gas phase experiments with its own cluster generation technique are important for the formation mechanism of endohedral metallofullerene. The precursor clusters could be directly examined only with these experimental approaches. Depending on the metal element and cluster source conditions, variety of structures of metal-carbon binary clusters can be generated and examined such as small cage endohedral metallofullerene $U@C_{28}$ [19], Met-Cars M_8C_{12} (M = Ti, V, Zr, Hf, Nb, Cr, Fe, Mo) [20], nanocrystal $Ti_{14}C_{13}$ [21], and heterofullerene NbC_{59} [22]. The formation process of SWNTs (single wall carbon nanotubes) [23-25] may be critically controlled with some metal-carbon binary clusters [26]. In addition to these theoretical interests, the formation mechanism of endohedral metallofullerene has the practical importance, since the more efficient production is desired for expected applications in medical and engineering field. The yield of the endohedral metallofullerene is much lower than 1 % except for the Dorn's TNT (trimetallic nitride template) type endohedral fullerenes such as $Sc_3N@C_{80}$ [27, See Chapter 13].

In this chapter, mass spectroscopic experiments are reviewed with an emphasis on the formation mechanism of endohedral metallofullerene and small metal-carbon binary clusters as the precursors. After the introduction of the generation technique of metal-carbon binary clusters with the laser vaporization supersonic expansion cluster beam source [28], FT-ICR spectroscopy [29,30] and ion mobility experiments [31-33] are discussed. In addition to these experimental works, direct molecular dynamics simulations of cluster growth process in Sc/C, La/C, and Ni/C mixed systems [29] are discussed in order to show the visual hints of the growth mechanism. Those classical molecular dynamics simulations with the Brenner potential [34] for carbon-carbon interaction and new metal-carbon interaction potentials [35] can reproduce the important precursors of the growth process. Here, the metal-carbon classical potential was made of the nearly covalent bonding term and the Coulombic potential term due to the charge transfer from the metal atom to the carbon clusters. At the end of the chapter, mass-spectroscopic experiments about small endohedral metallofullerene, Met-

Cars, and heterofullerene are reviewed.

2. GENERATION AND MEASUREMENT OF METAL-CARBON BINARY CLUSTERS

2.1 Generation of metallofullerene by cluster source

In most of mass spectroscopic studies, the cluster ion beam is generated by the so-called “Smalley-type” laser-vaporization supersonic-expansion cluster beam source [36]. An example of the latest version of the cluster beam source is shown in Figure 1 [29,30]. Here, the original design of this “mini-source” was developed by Smalley group [28] for the direct connection to the FT-ICR apparatus. A solid target disk, which can be rotated and translated, is vaporized by the focused beam of Nd: YAG laser (2nd Harmonics) while timed pulsed gas is injected to the nozzle. For the generation of endohedral metallofullerene clusters, metal-doped graphite disk is used as the ‘target disk’. The same material as for the macroscopic generation of metallofullerene by laser-furnace or arc-discharge methods can be used. The metal-graphite composite material is usually prepared by mixing the metal oxides powder such as La_2O_3, graphite powder and graphite cement in the specific ratio (typically a few atomic % of metal) and subsequent baking at about 1500 °C. The metal-graphite composite rods for typical percentage of typical metal elements are commercially available [37].

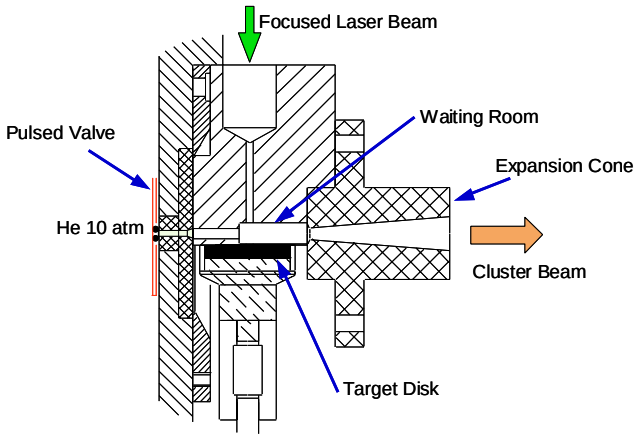

Figure 1. The Laser-vaporization supersonic-expansion cluster beam source [29,30].

With the commercial supersonic nozzle, very short (about 50 μs)

pulsed helium carrier gas is injected to the nozzle. When the gas pressure is increasing in the nozzle, Q-switched vaporization laser about 10 mJ/pulse focused to about 1 mm diameter spot is fired. In the atmosphere of helium gas, vaporized atoms condense to clusters, and then, are carried and cooled by the supersonic expansion of helium gas. The design of "waiting room" area just before the expansion is important for the control of growth clusters after the vaporization [28].

The design in Figure 1 was initially optimized for relatively large silicon clusters (such as Si_{30} through Si_{60}), germanium clusters and carbon clusters [28]. The generated cluster size distribution and probably isomer distribution are critically dependent on the timing of laser shot compared with the pulsed gas trigger and laser fluence and laser focus size. And, the "waiting room" design is also important for the well-annealed cluster generation. This part can be sometimes replaced with longer straight tube in cooling block [38] or electrical discharge heating followed by a long extender for cooling [39].

It should be noted that the cluster size and isomer distribution of each research group may be considerably different from another, because the detailed design of cluster beam source are not usually common.

The cluster beam is skimmed to the analyzing chamber with reflectron TOF, FT-ICR, or ion mobility apparatus. Since the reflectron TOF is well known, FT-ICR and ion mobility experiments are introduced in next sections.

2.2 FT-ICR mass spectrometer

FT-ICR (Fourier transform ion cyclotron resonance) mass spectrometer is unique and powerful apparatus for the clusters studies. Especially for metal-carbon binary cluster, the high mass resolution of FT-ICR is convenient for the assignment of complicated mass signals. Furthermore, the mass-selected reaction experiments [29,30,40], laser photodissociation experiments [4,19], and CID (collision-induced dissociation) experiments [41] can be done while cluster ions are trapped in the ICR cell for a few minutes. A FT-ICR mass-spectrometer at The University of Tokyo [29,30] originally developed at Rice University [28] is shown in Figure 2.

The specific dimensions of the FT-ICR apparatus in Figure 2 are as follows. The ICR cell (4 sections of 42 mm I.D. 150 mm long cylinder) is placed in a stainless tube (SUS316) with 84 mm I.D. which penetrates the homogeneous 6 Tesla superconducting magnet commercially available for NMR. Two turbo-pumps ($300\,\ell/s$) fore-pumped by a smaller turbo-pump of $50\,\ell/s$ are placed at the floor in order to avoid the effect of strong magnetic field. The typical background pressure is 3×10^{-10} Torr.

The cluster beam generated outside of magnetic field at 'Cluster Source' is directly injected to the 6 Tesla superconducting magnet through a pulsed deceleration tube with which the mass range trapped in the ICR cell is roughly selected. Positive or negative cluster ions directly generated by the vaporization laser or the ionised neutral cluster can be probed. The injected cluster ions are trapped in the ICR cell between 'Front Door' and 'Back Door'. By exciting the cluster ions with SWIFT technique [42], the mass spectra can be obtained.

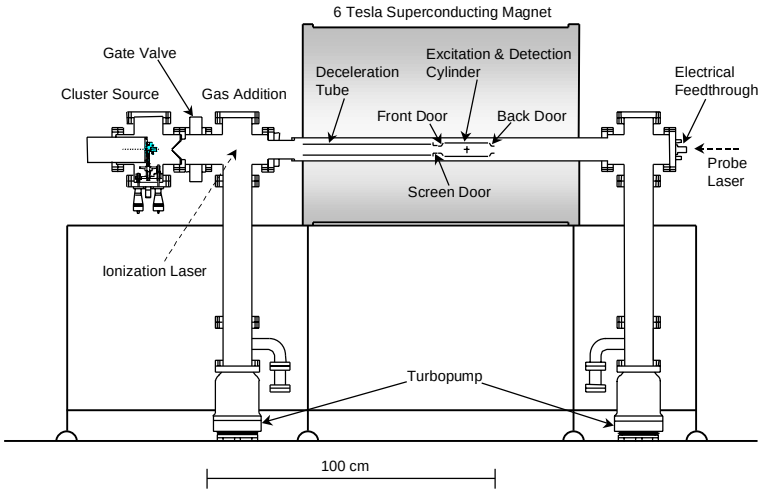

Figure 2. FT-ICR mass spectrometer directly connected with the cluster beam source [29,30].

An example of cluster mass spectrum measured with the FT-ICR is shown in Figure 3. The Sc-graphite composite disk with 0.8 atomic % Sc was used as the target disk. The mass window range by the pulsed deceleration tube during the injection was set to about the mass of C_{60}. Since the mass of Sc atom (44.956 amu) is nearly the 4 time of a carbon atom, signal of ScC_{2n-4}^+ appears just left side of C_{2n}^+ signal such as ScC_{56}^+ just left of C_{60}^+. In Figure 4, it is clearly seen that the mass distribution due to carbon isotopes are clearly distinguished. The pure carbon signals are C_{60}^+ and C_{70}^+ and small peaks of C_n^+ with an even number of carbon atoms. All signals in this range contained an even number of carbon atoms for pure carbon signals and for Sc atom containing signals. It is well known that the positive mass spectra of laser-vaporized carbon clusters C_n^+ have only even-numbered clusters for about $n \geq 30$ with enhanced intensity at C_{60}^+ and C_{70}^+. However, the enhancement of C_{60}^+ and C_{70}^+ in Figure 3 is much more than the pure graphite case. It seems that Sc atoms are somehow working as the catalyst, which enhances the formation of fullerene structure by pure carbon clusters.

The pure carbon clusters in the range in Figure 3 are probably almost completely fullerenes. Sc containing clusters also have an even number of carbon atoms, and ScC_{44}^+, ScC_{50}^+ and ScC_{60}^+ are dominant signals. Since these magic numbers, 44, 50 and 60 are the same as empty fullerene [39], the carbon structure is expected to be the fullerene structure. In summary, the mass spectrum suggests that all pure carbon clusters in this range have fullerene structure and all ScC_{2n}^+ are endohedral metallofullerene, $Sc@C_{2n}^+$.

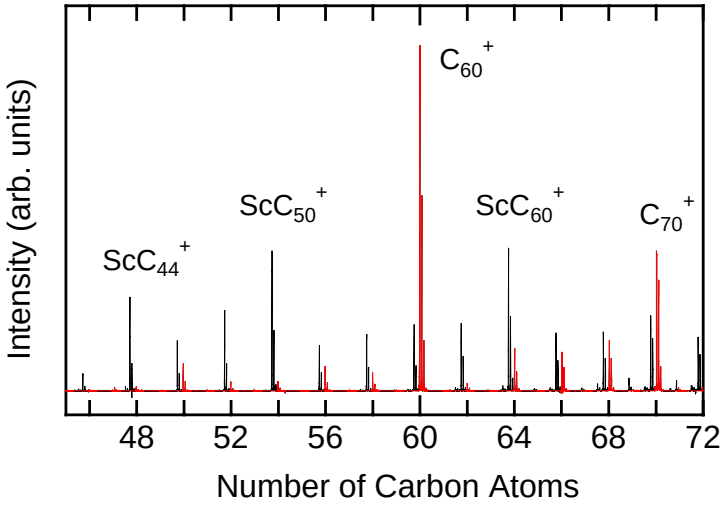

Figure 3. FT-ICR mass spectrum of Sc and carbon binary clusters.

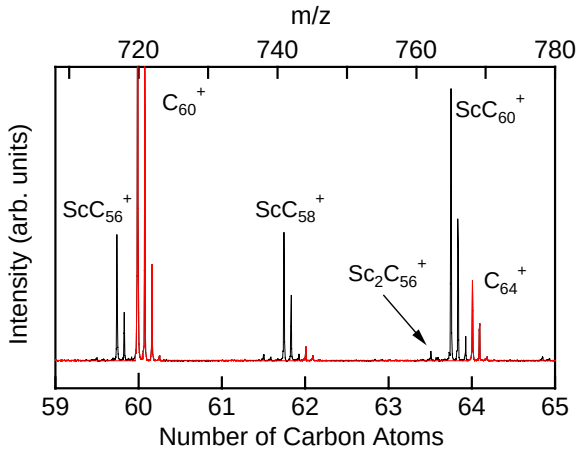

Figure 4. Expanded mass spectrum of Sc-C binary clusters in Figure 3.

In order to examine the structure of those clusters, reaction experiments and photo-dissociate experiments can be performed in FT-ICR framework. However, these assignments are always indirect.

2.3 Ion mobility (ion chromatography) measurements

Another powerful and unique spectroscopic apparatus is the ion mobility measurements employed for carbon clusters by Bowers et al. [7-9] and Jarrold et al. [10-12]. The ion chromatographic separation of isomers of carbon cluster cations into chains, rings, and fullerenes by Bowers et al. [7] was the very impressive work. Furthermore, the conversion of ring isomers to fullerene isomer or to large monocyclic ring by the annealing experiments [8,10-12] was so important in the discussion of fullerene formation mechanism. Later, Jarrold et al. [31-33] applied this technique for the endohedral metallofullerene.

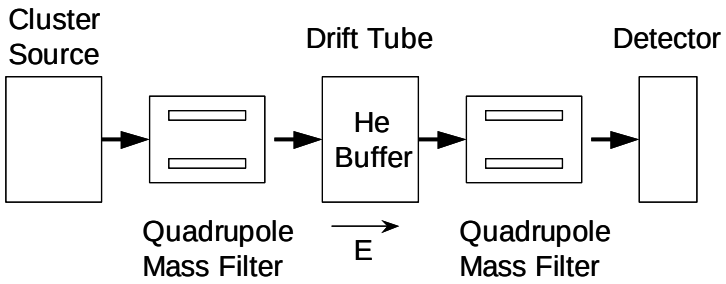

Figure 5. A schematic diagram of the tandem quadrupole drift tube apparatus [10].

A schematic diagram of the apparatus [10] in Jarrold group is shown in Figure 5. The laser vaporization cluster source is similar to the one in Figure 1. The cluster ion that exits the source is mass-selected with a quadrupole mass spectrometer [10] or a magnetic and electrostatic analyser [7] and injected into a drift tube containing about 5 Torr of helium buffer gas. After drift of ion clusters in a weak electric field about 10 V/cm, exiting time from the drift tube depends on the ion mobility in the helium gas. Upon exiting the drift tube, cluster ions are mass analysed by the quadrupole mass spectrometer and detected with an ion detector. Here, the injection energy to the drift tube can be varied from 5 eV up to around 400 eV. As the ions enter the drift tube, a fraction of their kinetic energy is converted into a cluster through collisions with the buffer gas. If the injection energy is large enough, the cluster may isomerise or fragment. Further collisions with the buffer gas cool the clusters to thermal temperature. The clusters then drift slowly across the drift tube for the mobility measurement.

The recent high-resolution ion mobility apparatus [43] with higher helium buffer gas pressure of 500 Torr and higher drift voltage of up to 14 kV has an order of magnitude higher resolution. Now the structural isomers of $Sc_2@C_{82}^+$ are resolved [44].

For pure carbon cluster cations, isomer distributions and abundant change as a function of cluster size were determined as follows [7]. The inverse mobility dependence is schematically shown in Figure 6 [32]. Linear chain structure was dominant for small clusters up to C_{10}. Near C_{10} planar monocyclic rings (ring I = ring Ib) appeared which gradually gave way to planar bicyclic rings (ring II) between C_{20} and C_{30}, followed by planar tricyclic rings (ring III, not shown in Figure 6). Then, the graphite (originally assigned as 3-D ring [7] later recognized as graphite [9,32]) began at about C_{30} as relatively small amount. Fullerene isomer appeared at C_{30} for the cations and dominated by C_{50}. For negative ions the planar multicyclic rings dominated to well above C_{60} [9]. Furthermore, the annealing experiments revealed the transformation of ring structure to fullerene structure [8].

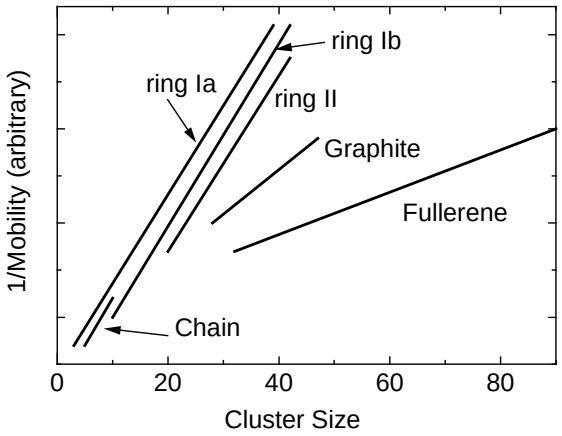

Figure 6. Inverse mobilities of LaC_n^+ isomers against the cluster size.

The experimental results for LaC_n^+ case [32] are schematically drawn in Figure 6. The results of metal-containing carbon clusters were similar to the pure carbon case. Three different metal-containing carbon rings (ring Ia, ring Ib, and ring II), metal-containing graphite sheets, and metallofullerene were resolved. The difference from C_n^+ case was that no linear chain was observed because the La could connect the each end of a chain. The assigned geometries were La inserted into carbon ring (ring Ia), a La inside a carbon ring (ring Ib), and various LaC_n and C_m rings fused together (ring II). The relative abundance of the graphite sheet and the metallofullerene were substantially larger than for the pure carbon clusters. Both endohedral and

non-endohedral metallofullerene were resolved. LaC_n^+ fullerenes with $n \geq 36$ were endohedral, while $29 \leq n \leq 35$ were non-endohedral. For large clusters, fullerenes and graphite sheets were formed when the rings were annealed. The efficiency of this annealing process was much larger than in the pure carbon system, although the activation energies appeared to be approximately the same.

3. MASS SPECTRA OF ENDOHEDRAL METALLOFULLERENE

3.1 Positive mass spectra for Ca, Sc, Y, La, and Lanthanides

The FT-ICR mass spectra of metal-carbon binary clusters are compared in Figure 7 for Sc, Y, and La doped cases [29]. The starting materials were composite disks of Sc/C, Y/C, and La/C optimized for the macroscopic generation of endohedral metallofullerene (nominal atomic mixing rates are Sc 0.8%, Y: 0.8%, or La: 0.8%). All of these samples were commercially supplied [37]. In the mass range shown in Figure 7, binary clusters YC_n, LaC_n shows the similar tendency as for ScC_n discussed in Figure 3 and Figure 4. Only difference was the relative amount of pure carbon signals. There was only weak C_{60} signal of pure carbon cluster in the Y doped case. And, almost no pure carbon signal was observed in La doped case. All clusters had one La atom in the mass range in Figure 7.

By slightly changing the cluster source condition to higher pressure in the nozzle, the right hand panel of Figure 7 was obtained. Here, di-metallic clusters became more dominant than the lower pressure case in the left panel. Typical clusters like $M_2C_{70}^+$ and $M_2C_{82}^+$ were detected for Sc and Y in addition to the monatomic clusters. But, the di-metallic clusters were not detected for La-C system. Probably higher pressure and higher mass range must be explored for La-C system. Apparently, the minimum cage size for Sc and Y were $Sc_2C_{54}^+$ and $Y_2C_{64}^+$, respectively [29]. These thresholds agree well with the recent similar experimental results that $Sc_2C_{52}^+$ and $Y_2C2_{62}^+$ are the minimum di-metallofullerene [45]. However, another recent experiment [46] showed the threshold of 70 atoms both for Sc and Y. The reason for the difference is probably the conditions in the cluster beam source.

In addition to those metal atoms, Gd, Ce did show almost the same results as La case [29]. As a summary, for all cases of Sc,-C Y-C, La-C, Gd-C and Ce-C strong MC_{2n}^+ signal in the range of $36 \leq 2n$ with intense magic

numbers at MC_{44}^+, MC_{50}^+ and MC_{60}^+ were detected.

For C-Ca case, this feature was still valid but CaC_{60}^+ was very much enhanced [29].

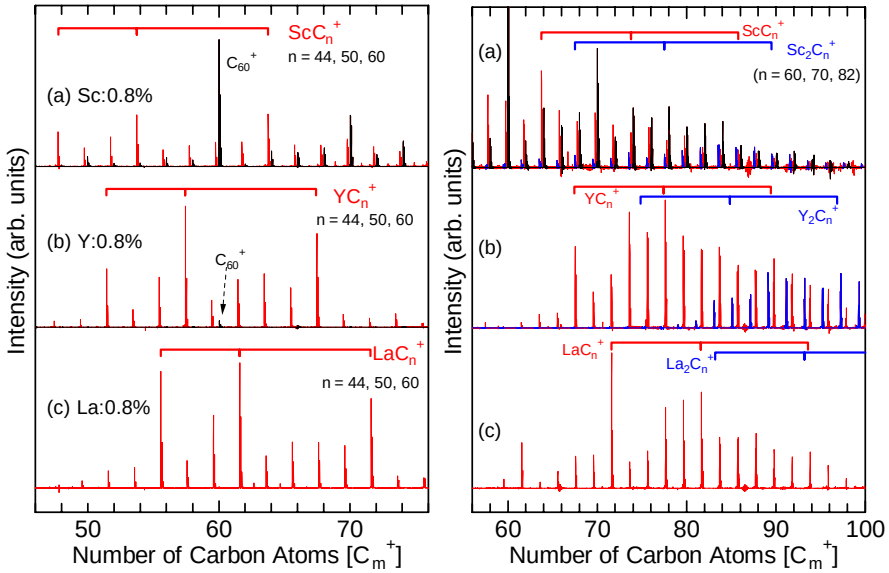

Figure 7. FT-ICR positive mass spectra from Sc-, Y-, and La-doped graphite disk. Left and right hand panels are with lower- and higher-pressure condition, respectively.

3.2 Negative mass spectra and reaction experiments

Even though LaC_{2n}^+ ($36 \leq 2n$) signal was so dominant in Figure 7, amount of pure carbon clusters C_{2n} may not be negligible compared to LaC_{2n} for neutral clusters because the ionization potential of metal-carbon binary clusters are expected to be considerably lower than pure carbon clusters. Since negative clusters are believed to reflect the abundance of neutral clusters, negative clusters will be examined in this section. For La-C case, negative and positive clusters spectra are compared in Figure 8 [30]. The negative cluster distribution in Figure 8 (b) could be simply recognized as the superposition of small pure carbon C_m^- clusters up to about C_{60}^- with LaC_{2n}^- cluster distribution similar to positive clusters. The distribution of pure carbon clusters seems to be the same as the typical negative mass spectrum obtained from pure-graphite sample. Small even-odd alternations in pure carbon clusters C_m^- were an artifact due to the hydrogen contamination [30]. Here, it should be noted that most of LaC_n^- has a even number of carbon atoms and LaC_{44}^- was dominant as positive mass spectra.

This situation can be recognized that with La atom, the metal-carbon cluster can very efficiently convert to the fullerene structure as suggested in the ion mobility experiments [32].

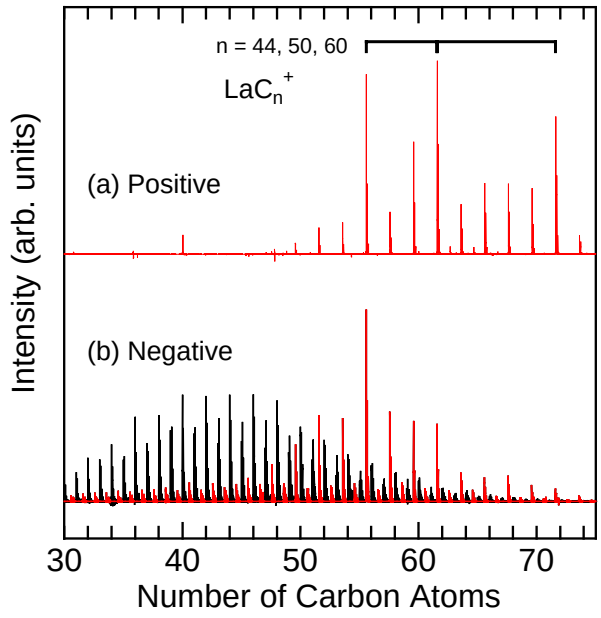

Figure 8. Mass spectra of positive and negative clusters generated by the laser vaporization of La doped graphite material

The chemical reaction experiment with nitric oxide was performed to determine if the La was in the endohedral position [30]. The following is the typical chemical reaction procedure in the FT-ICR experiment:

Cluster beam is injected in 10 Hz for 10 s to the ICR cell. The deceleration voltage roughly selects size range of cluster ions.

The kinetic energy of clusters is thermalized with room temperature argon gas at 10^{-5} Torr for 10 s.

Unwanted clusters are over-excited and excluded from ICR cell by SWIFT (Stored Waveform Inverse Fourier Transform) [42] excitation.

Remaining clusters are thermalized with room temperature argon gas at 10^{-5} Torr for 10 s.

Nitric oxide gas is injected to the cell by 10 Hz pulsed valve for a fixed period. The pulse value is adjusted so that the pressure at the ICR cell chamber becomes at 10^{-5} Torr for unreactive clusters and 10^{-7} Torr for reactive clusters.

After pumping out for about 8 to 10 s, cluster ions are excited to detect the mass spectrum.

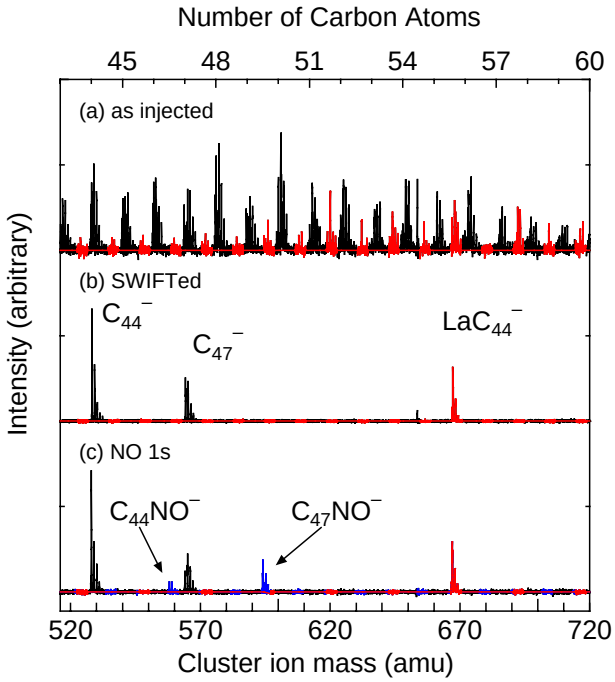

Figure 9. FT-ICR reaction experiment. (a) The mass distribution as injected to the FT-ICR. (b) C_{44}^-, C_{47}^-, and LaC_{44}^- were selected with the SWIFT technique. (c) After the reaction with NO for 1 s.

Figure 9 compares the reactivity of La-C binary cluster LaC_{44}^- to typical odd and even numbered pure carbon clusters C_{44}^- and C_{47}^-. After 1 s reaction with NO, reaction of C_{47} and a little bit of C_{44} were observed as in Figure 9(c). However, the reaction of LaC_{44} was not observed. In general, it is expected to be more reactive if a metal atom is exposed to NO. The much less reactive LaC_{44}^- strongly suggests that La atom is inside the carbon cage. Furthermore, since La-C binary clusters with odd number of carbon atoms were much less abundant than even-numbered carbon atoms, it can be speculated that LaC_{2n} such as LaC_{44} are much better annealed than pure carbon clusters.

3.3 Clusters with even number of carbon atoms

A careful examination of isotropic mass distribution of negative carbon clusters in Figure 9 shows that about half of odd-numbered pure

carbon clusters C_{2n-1}^- were contaminated with a hydrogen atom [30]. Then, a careful observation of C_{47}^- in Figure 9 leads to an interesting results. The signal marked as C_{47}^- in Figure 9 is actually about 1:1 mixture of C_{47}^- and $C_{47}H^-$. After the exposure of NO, C_{47}^- reacted completely as $C_{47}NO^-$ but $C_{47}H^-$ did not react much in Figure 9(c) [Expansion of mass scale is necessary]. These experimental results were completely explained by the following discussions [30].

The positive ion mass spectra with enhanced signal of clusters with an even number of carbon atoms was connected to the geometrical structure of fullerene as follows. For a closed polyhedral structure, there is a following Euler's relation between number of faces *f*, number of edges *e*, number of vertices *v*.

$$f + v = e + 2 \tag{1}$$

There are additional relations between number of pentagons f_5 and number of hexagons f_6 for a fullerene.

$$2e = 5f_5 + 6f_6, \quad 3v = 5f_5 + 6f_6 \tag{2}$$

As a result, it is well known that the number of pentagon is always 12 and number of total atoms is even as

$$f_5 = 12, \; v = 20 + 2f_6 \tag{3}$$

However, if we consider that all atoms had three bonds (no dangling bonds), it can be directly derived that number of atoms must be even regardless of size of faces. The condition that all atoms had three bonds can be expressed as

$$e = \frac{3}{2}v. \tag{4}$$

Only with this condition (without the assumption in eq. (2)) Euler's theorem can be rewritten to

$$v = 2f - 4, \tag{5}$$

which means that number of atoms (vertices) must be even.

Considering the number of atoms with a dangling bond (atoms with only 2 bonds) as v_2, with number of atoms with 3 bonds v_3, the relation in eq.

(4) is modified to

$$e = \frac{3}{2} v_3 + v_2 . \tag{6}$$

Then, the equation (5) is modified to

$$v = 2f - 4 + v_2 . \tag{7}$$

This means that when total number of atoms in a cluster $v = v_2 + v_3$ is even, number of atoms with a dangling bond v_2 is even, and when v is odd, v_2 is odd. Since odd numbered clusters had at least one dangling bond, contamination with a hydrogen atom can be enhanced. The reactivity of NO to pure carbon clusters can be interpreted that NO reacted to the local site with the dangling bond. And, a hydrogen atom attached to odd-numbered cluster can block the attack of NO [30].

It is important to note that the even-numbered mass distribution does not directly mean the fullerene structure (6- and 5-membered rings), but many different isomers with relatively small energy difference does exist. The molecular dynamics simulation at high temperature at 2500 K could anneal carbon clusters with 30 to 60 atoms to finally fullerene structure [47,48]. Here, starting from a random structure, most of clusters tried to reduce the number of dangling bonds. At this stage, even numbered clusters always had 0, 2, 4, … atoms with a dangling bond (an atom with 2-bonds), and odd numbered clusters had 1, 3, 5, … atoms with a dangling bond. Finally, at least one dangling bond remained for odd numbered clusters. When number of atoms is even, all faces became pentagons and hexagons, and finally transformed to IPR structure through Stone-Wales transformations.

4. MOLECULAR DYNAMICS SIMULATIONS

4.1 Simulation technique

The principal technique of the classical MD simulation is described in our previous simulations of empty fullerene [47,48], and endohedral metallofullerene [29,35]. For the carbon-carbon potential the modified Brenner potential [34] was used. In addition, we have constructed the classical potential function between carbon clusters and several metal atoms (La, Sc and Ni) for the molecular dynamics simulation of generation of

endohedral metallofullerene [35] based on DFT calculations of small metal-carbon binary clusters. The metal-carbon multi-body potential function was expressed as functions of carbon coordination number of a metal atom in the similar framework as Brenner potential. The total potential energy was expressed as the sum of binding energy E_b as follows.

$$E_b = V_R + V_A + V_C \tag{8}$$

$$V_R = f(r_{ij}) \frac{D_e}{S-1} \exp\left\{-\beta\sqrt{2S}(r_{ij} - R_e)\right\} \tag{9}$$

$$V_A = -f(r_{ij}) \cdot B^*_{ij} \frac{D_e S}{S-1} \exp\left\{-\beta\sqrt{2/S}(r_{ij} - R_e)\right\} \tag{10}$$

$$V_C = -f(r_{ij}) \frac{e^2}{4\pi\varepsilon_0} \frac{c_{\mathrm{C}} c_{\mathrm{M}}}{r_{ij}} \tag{11}$$

Here, r_{ij}, V_R and V_A denoted the distance between metal *i* and carbon *j*, Morse-type repulsive and attractive terms, respectively. The Coulomb term V_C was applied only to the La-C and Sc-C interactions with considerable charge transfer from the metal to carbon atoms.

The coordinate number of the metal atom N^{C} was defined using the cut-off function *f*(*r*). Both the pre-factor to the attractive term B^*_{ij} and the electric charge *c* were expressed as functions of the coordinate number N^{C}. Considering the typical situation that a metal atom was surrounded by several carbon atoms, the effect of the bond angle between M-C bonds was ignored.

$$f(r) = \begin{cases} 1 & (r < R_1) \\ \left(1 + \cos\dfrac{r - R_1}{R_2 - R_1}\right)/2 & (R_1 < r < R_2) \\ 0 & (r > R_2) \end{cases} \tag{12}$$

$$N^{\mathrm{C}} = 1 + \sum_{\text{carbon } k(\neq j)} f(r_{ik}) \tag{13}$$

$$B^* = \left\{1 + b(N^{\mathrm{C}} - 1)\right\}^{\delta} \tag{14}$$

$$c_{\mathrm{M}} = 3 - \exp(-k_1 N^{\mathrm{C}} + k_2),\ c_{\mathrm{C}} = c_{\mathrm{M}} / N^{\mathrm{C}} \tag{15}$$

Potential parameters obtained by fitting to several DFT calculations of small metal-carbon clusters are listed in Table 1. Metal-metal interaction potentials were also constructed in the similar form [35].

Table 1 Potential parameters for metal-carbon interactions.

	D_e (eV)	S	β (1/Å)	R_e (Å)	R_1 (Å)	R_2 (Å)	b	δ	k_1	k_2
La-C	4.53	1.3	1.5	2.08	3.2	3.5	0.0854	-0.8	0.0469	1.032
Sc-C	3.82	1.3	1.7	1.80	2.7	3.0	0.0936	-0.8	0.0300	1.020
Ni-C	3.02	1.3	1.8	1.70	2.7	3.0	0.0330	-0.8	-	-

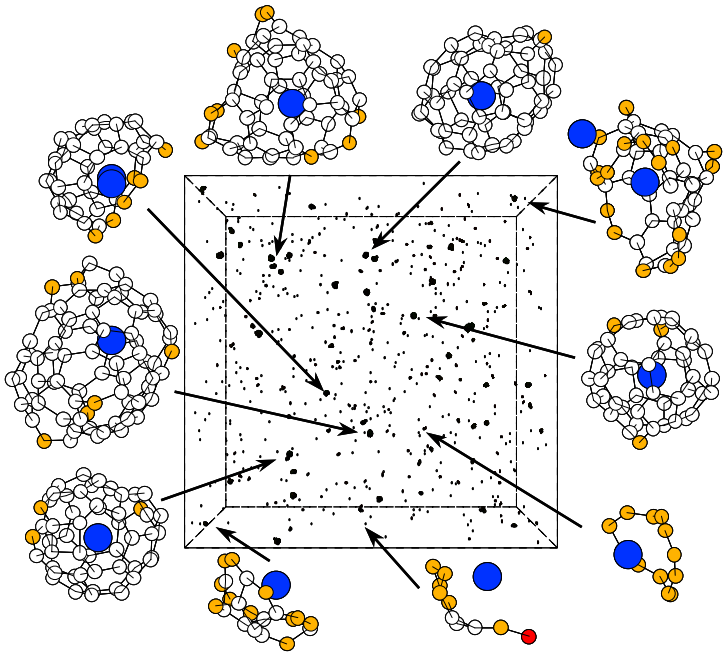

Figure 10. Snapshot of MD simulation of growth process of La-C clusters, 3000 K, 3ns. Dark circle and gray circle mean La atom and carbon atom with a dangling bond, respectively.

4.2 L-C binary system

The growth process of metal-carbon binary clusters was simulated with the same technique as in [35] but 5 times larger system. As the initial condition, the completely random vapor mixture of 2500 carbon and 25 La atoms were allocated in a 585 Å cubic fully periodic simulation cell. The high density of the system was compensated with the special temperature control method at T_c = 3000 K. Figure 10 shows a snapshot after 3 ns molecular dynamics calculation starting from the random gas phase initial condition. Several endohedral metallofullerene are observed in Figure 10. As shown in the gray circle, there are several atoms, which have the dangling bonds even for the nice endohedral fullerenes. The annealing of the structure is largely ignored in this simulation [48]. The growth process leading to the imperfect endohedral metallofullerene was traced [35].

Figure 11 shows the growth process of typical La attached clusters in the simulation; (a) a La containing caged cluster La@C_{73} observed at t = 3000 ps, and (b) a La attached cluster LaC_{17} observed at t = 1600 ps. The vertical width and horizontal length denote the cluster size and time, respectively. For example, in Figure 11 (a), the LaC_5 and C_{13} cluster independently existed each other, coalesced at about 530 ps, and the LaC_{19} was formed after the addition of a carbon atom at about 550 ps.

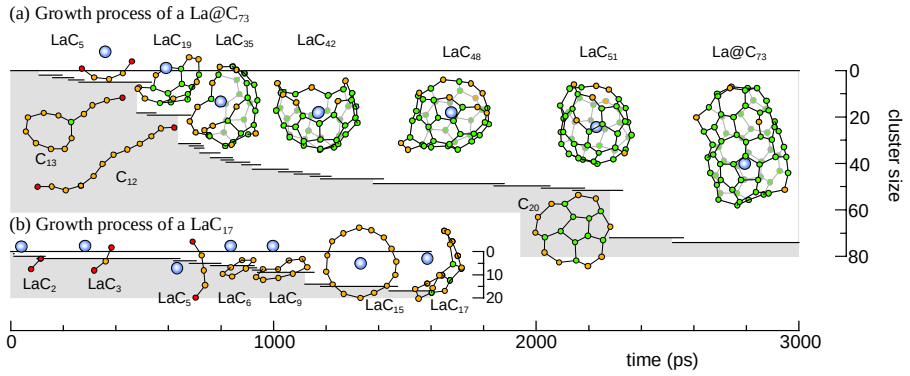

Figure 11. Growth process of La attached clusters: (a) La@C_{73} and (b) La@C_{17}.

The remarkable difference from our simulation for empty fullerene [47] was clearly observed in the precursors in the size range of LaC_{19} to LaC_{51}. Since the La atom can be a nice nucleation site of carbon atoms, it can attract carbon atoms by Coulomb force in very much-organized manner. The open-cap appearance of carbon cluster form resembles to the ‘pentagon road’ fullerene formation model [18] proposed for empty fullerene. The cluster grew larger with closing the open-cap structure after LaC_{51}. In this

case, however, a collision with a large cluster of C_{20} prevented gradual growth and resulted in the formation of a caged cluster larger than La@C_{71}, and the La atom was almost encapsulated in the carbon cage. Considering the difference of time and temperature scale between the real phenomena and simulation, these hollow caged structures could have sufficient collision free annealing interval to form more sophisticated structures.

The precursor clusters are linear chain for pure carbon clusters up to about C_{10} but La attached cluster becomes ring structure or fan structure as in Figure 11(b). These rings were denoted as “ring Ia” in the ion mobility measurements [32]. With the increase of number of carbon atoms, “ring Ib” type like LaC_{15} appears. Then, the bowl type carbon structure may be close to the “ring II” type. Closed fullerene cage may be possible from about La@C_{40} with this simulation. Hence, the general idea of precursor cluster is well reproduced in these simple molecular dynamics simulations.

The tadpole structure observed by the high-resolution ion mobility apparatus [49] is observed in Figure 11 (a) as C_{13}.

4.3 Sc-C binary system

Clustering process with Sc atoms was simulated under the same condition as the previous section. Figure 12 shows the growth process of a ScC_{55} observed at t = 4000 ps. A remarkable difference of the process from La-C system is apparent for the structures of MC_n ($20<n<40$) because of the weaker Coulomb force. The cluster annealed to the 3-dimensional open cage structure around ScC_{43}, where the scandium atom moved around the open edge. The Sc atom slipped into the cage structure just before closing at around Sc@C_{54}. The random cage form of carbon clusters is almost the same as the case of our empty fullerene simulation. The effect of Sc atom is relatively weak to change the carbon structure.

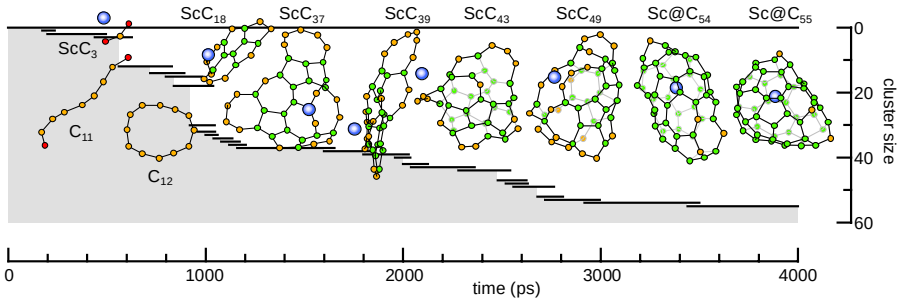

Figure 12. Growth process of Sc attached cluster, Sc@C_{55}.

The Sc atom was trapped inside in Figure 12 but the atom may stay

exohedoral when the carbon cage is closed. Then, the Sc atom have to react away in the later process. Or, there may be possibility that Sc atom will leave the carbon cluster by a collision with some clusters when the carbon cage is almost ready. Then, the considerable enhancement of pure carbon growth toward cage structure can be explained.

4.4 Ni-C binary system

Nickel atom, which is important catalytic metal for the SWNTs formation, is also examined. As shown in Figure 13, the growth process is very similar to that for Sc attached cluster. However, at the final stage, the Ni atom preferred to attach at the large defect of the caged structure such as large rings of more than 7 or 8 member ring, and frequently moved in and out of the carbon cage.

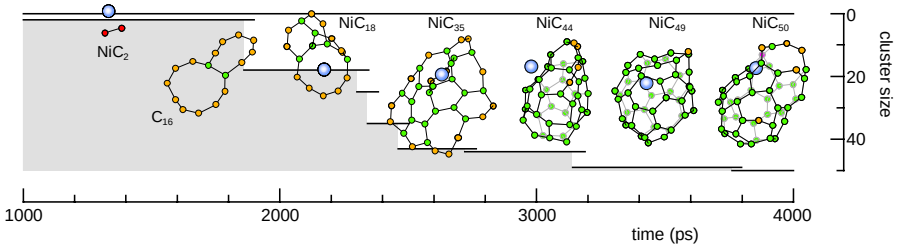

Figure 13. Growth process of Ni attached cluster, Ni@C_{50}.

5. MET-CARS, HETEROFULLERENE AND MORE

By substituting one or more cage carbon atom of fullerene with another atom, heterofullerene can be formulated. The first demonstration of such heterofullerene, $C_{59}B$ and $C_{58}B_2$, was obtained by the FT-ICR experiments in Smalley's group [50]. Here, a graphite disk doped with Boron nitride (BN) was laser-vaporized. The partial success of macroscopic extraction of $C_{59}B$ and $C_{69}B$ through the arc-discharge generator was reported later [51]. Until now the only purely isolated and characterized heterofullerene is $C_{59}N$ or aza[60]fullerene [52]. Unstable heterofullerene with Si atom SiC_n ($n \geq 30$) were demonstrated by the mass-spectroscopic experiments by Shinohara et al. [53] through the laser vaporization of so-called bulk siliconized graphite with atomic ratios of Si/C (1/100) sample. Ion mobility experiments [54] and laser photo-fragmentation experiments [55] confirmed the heterofullerene structure.

The heterofullerene with metal atoms were also distinguished by the mass-spectroscopic studies [22] as NbC_n^+ (n = 28-50). And, cage substituted fullerene with such metal atoms such as Fe, Co, Ni, Rh were reported [56]. The externally bound metallofullerene such as FeC_{60}^+ [41] can be made by the gas phase reaction of C_{60} and Fe ion. Furthermore, more recent examples of mass-spectroscopic products that had not isolated are Met-Cars proposed by Castleman et al. [20]. The trimetallic nitride endohedral fullerene such as $Sc_3N@C_{80}$ by Dorn et al. [27] was exceptions. Even though the initial note about this fantastic new species was as the mass peak of m/z = 1,109, it was already extracted sample.

Coming back to the endohedral metallofullerene, the mass-spectroscopic measurements suggested wider varieties of metal atoms and cage sizes than successfully isolated metallofullerene. The isolated metallofullerene are usually $M@C_{82}$ type with (M = Sc, Y, La, Ce, Pr, Gd...). Di-metal endohedral fullerene seems to favor C_{84} cage such as $Sc_2@M_{84}$, though other cage products were isolated such as $Sc_2@C_{74}$, $Sc_2@C_{82}$, $La_2@C_{80}$, $Y_2@C_{82}$ [57]. And, 3 metal atoms $Sc_3@C_{82}$, and 4 metal atoms $Sc4@C_{82}$ can be isolated. Except for the very recent IPR violating metallofullerene $Sc_2@C_{66}$ [58] and $Sc_3N@C_{68}$ [59], the fullerene cage size were larger than C_{70}. Until the recent isolation of $Er@C_{60}$ [60] and $Eu@C_{60}$ [61], the existence of $M@C_{60}$ has been often doubted. Usually, $M@C_{60}$ is the most dominant peak in the most mass spectroscopic results either from the graphite composite disk or arc-discharge generated soot. The mass spectroscopic results showed much smaller endohedral metallofullerene such as $U@C_{28}$ [19, 62] in very early time. Some more details of metallofullerene in small cage such as $M@C_{44}$, $M@C_{50}$, and $M@C_{60}$ [29,30,45] shown in Figure 14 have been discussed in this chapter.

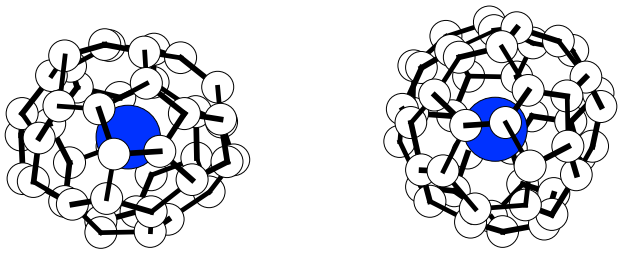

(a) $La@C_{44}$ (b) $La@C_{50}$

Figure 14. Annealed structures of (a) $La@C_{44}$ and (b) $La@C_{50}$

Depending on the metal element and mixing ratio, metal-carbon cluster makes very different and interesting structures. The rare earth metals

such as Ca, Sr, Ba, Sc, Y, La and lanthanides could be encapsulated inside the fullerene cage. The early transition metals, Ti, V Zr, Hf, Nb, Cr, Fe, Mo resulted the Met-Cars [20,21,38,63,64]. On the other hand, late transition metals, Ni, Pd, Pt are required to generate the SWNTs [23] in the laser-oven [24] or arc discharge techniques [25]. For the more efficient production of SWNTs, some combinations such as Ni-Co, Ni-Fe, Pd-Rh and Pr-Ir are used. Finally, the cage substituted fullerenes should be recalled: Nb, Fe, Co, Ni, Rh are discussed.

Probably, the systematic studies of those metal elements such as the possibility of endohedral metallofullerene [62] would be very useful. Wang et al. started the systematic high-resolution UPS studies of MC, MC_2, MC_3... [65]

6. SUMMARY

Mass spectroscopic experiments related to endohedral metallofullerene are reviewed. The formation mechanism of endohedral form of metallofullerene is discussed with FT-ICR mass spectroscopic results, and ion mobility results. The different geometrical structures of metal-carbon binary clusters depending on metal atoms are summarized. Importance of the charge transfer and Coulombic attractive potential force between metal atom and carbon cluster is emphasized. A classical molecular dynamics simulation demonstrating this idea is outlined. The electro-negativity can be the first order parameter to determine if a metal atom comes inside the carbon cage. Some other structure of metal-carbon binary clusters such as Met-Cars, heterofullerene with a metal atom cooperated in the carbon cage, small cage endohedral metallofullerene such as M@C_{44}, M@C_{50}, and M@C_{60} are discussed.

ACKNOWLEDGMENTS

The author would like to thank Dr. Masamichi Kohno (AIST) and Shuhei Inoue, Yasushi Shibuta, and Yasutaka Yamaguchi (The University of Tokyo) for their help in experiments and molecular dynamics simulations. Part of this work was supported by Grant-in-Aid for Scientific Research (B) (No. 12450082 and No. 13555050) from the Ministry of Education, Culture, Sports, Science and Technology, Japan.

REFERENCES

1. Kroto, H. W., Heath, J. R., O'Brien, S. C., Curl, R. F. and Smalley, R. E., Nature 1985, 318, 162.
2. Heath, J. R., O'Brien, S. C., Zhang, Q., Liu, Y., Curl, R. F., Kroto, H. W., Tittel, F. K. and Smalley, R. E., J. Am. Chem. Soc. 1985, 107, 7779.
3. O'Brien, S. C., Heath, J. R., Curl, R. F. and Smalley, R. E., J. Chem. Phys. 1988, 88, 220.
4. Weiss, F. D., Elkind, J. L., O'Brien, S. C., Curl, R. F. and Smalley, R. E., J. Am. Chem. Soc. 1988, 110, 4464.
5. Curl, R. F. and Smalley, R. E., Science 1988, 242, 1017.
6. Yang, S., Taylor, K. J., Craycraft, M. J., Conceicao, J., Pettiette, C. L., Cheshnovsky, O., Smalley, R. E., Chem. Phys. Lett. 1988, 144, 431.
7. von Helden, G., Hsu, M.-T., Gotts, N., and Bowers, T., J. Phys. Chem. 1993, 97, 8182.
8. von Helden, G., Gotts, N. G. and Bowers, M. T., Nature 1993, 363, 60.
9. Gotts, N. G., von Helden, G., Bowers, M. T., Int. J. Mass Spectrom. Ion Process 1995, 217.
10. Hunter, J. M., Fye, J. L., and Jarrold, M. F., J. Chem. Phys. 1993, 99, 1785.
11. Hunter, J., Fye, J. and Jerrold, M. F., Science 1993, 260, 784.
12. Hunter, J. M., Fye, J. L., Roskamp, E. J., and Jarrold, M. F., J. Phys. Chem. 1994, 98, 1810.
13. Chai, Y., Guo, T., Jin, C., Haufler, R. E., Chibante, L. P. F., Fure, J., Wang, L., Alford, J. M. and Smalley, R. E., J. Phys. Chem. 1991, 95, 7564.
14. Shinohara, H., Sato, H., Saito, Y., Ohkohchi, M. and Ando, Y., J. Phys. Chem. 1992, 96, 3571.
15. Kikuchi, K., Suzuki, S., Nakano, Y., Nakahara, N., Wakabayashi, T., Shiromaru, H., Saito, K., Ikemoto, I. and Achiba, Y., Chem. Phys. Lett. 1993, 216, 23.
16. Takata, M., Umeda, B., Nishibori, E., Sakata, M., Saito, Y., Ohno, M. and Shinohara, H., Nature 1995, 377, 46.
17. Krätschmer, W., Lamb, L.D., Fostiropoulos, K. and Huffman, D. R., Nature 1990, 347, 354.
18. Haufler, R. E., Chai, Y., Chibante, L. P. F., Conceicao, J., Jin, C., Wang, L.-S., Maruyama, S. and Smalley, R. E., Proc. Mat. Res. Soc. Symp. 1991, 206, 627.
19. Guo, T., Diener M., Cai, Y., Alford, M. J., Haufler, R. E., McClure, S. M., Ohno, T., Weaver, J. H., Scuseria, G. E., and Smalley, R. E., Science 1992, 257, 1661.
20. Guo, B. C., Kerns, K. P., and Castleman, Jr, A. W., Science 1992, 255, 1411.
21. Pilgrim, J. S., Duncan, M. A., J. Am. Chem. Soc., 1993, 115, 6958.
22. Clemmer, D. E., Hunter, J. M., Shelimov, K. B. and Jarrold, M. F., Nature 1994, 372, 6503.
23. Iijima, S. and Ichihara, T., Nature 1993, 363, 603.
24. Thess, A., Lee, R., Nikolaev, P., Dai, H., Petit, P., Robert, J., Xu, C., Lee, Y. H., Kim, S. G., Rinzler, A. G., Colbert, D. T., Scuseria, G. E., Tomának, D., Fischer, J. E., and Smalley, R. E., Science 1996, 273, 483.
25. Journet, C., Maser, W. K., Bernier, P., Loiseau, A., de la Chapelle, M. L., Lefrant, S., Deniard, P., Lee, R., and Fisher, J. E., Nature 1997, 388, 756.
26. Maruyama, S., Application of Fullerenes 2001, Ed. E. Osawa, Kluwer, Dordrecht, in press
27. Stevenson, S., Rice, G., Glass, T., Harich, K., Cromer, F., Jordan, M. R., Craft, J., Hadju, E., Bible, R., Olmstead, M. M., Maitra, K., Fisher, A. J., Balch, A. L. and Dorn, H. C., Nature 1999, 401, 55.
28. Maruyama, S., Anderson, L. R. and Smalley, R. E., Rev. Sci. Instrum. 1990, 61, 3686.
29. Maruyama, S., Yamaguchi, Y., Kohno, M. and Yoshida, T., Fullerene Sci. Technol. 1999, 7, 621.

30. Maruyama, S., Kohno , M. and Inoue, S., Fullerene 2000: Chemistry and Physics of Fullerenes and Carbon Nanomaterials 2000, 309.
31. Clemmer, D. E., Shelimov, K. B. and M. F. Jarrold, Nature 1994, 367, 718.
32. Shelimov, K. B., Clemmer, D. E., and Jarrold, M. F., J. Phys. Chem. 1995, 99, 11376.
33. Shelimov, K. B., Jarrold, M. F., J. Am. Chem. Soc. 1996, 118, 1139.
34. Brenner, D. W., Phys. Rev. B 1990, 42, 9458.
35. Yamaguchi, Y. and Maruyama, S., Euro. Phys. J. D 1999, 9, 385.
36. Dietz, T. G., Duncan, M. A., Powers, D. E. and Smalley, R. E., J. Chem. Phys. 1981, 74, 6511.
37. Toyo Tanso Co. Ltd. (Osaka). http://www.toyotanso.co.jp/
38. Sakurai, H. and Castleman, Jr., A. W., J. Phys. Chem. A 1998, 102, 10486.
39. Handschuh, H., Ganteför, G., Kessler, B., Bechthold, P. S., Eberhardt, W, Phys. Rev. Lett. 1995, 74, 1095.
40. McElvany, S. W., J. Phys. Chem. 1992, 96, 4935.
41. Roth, L. M., Huang, Y. Schwedler, J. T., Cassady, C. J., Ben-Amotz, D., Kahr, B., and Freiser, B. S., J. Am. Chem. Soc. 1991, 113, 6298.
42. Marshall, A. G. and Verdun, F. R., Fourier Transforms in NMR, Optical, and Mass Spectrometry, Elsevier, Amsterdam 1990.
43. Dugourd, Ph., Hudgins, R. R., Clemmer, D. E., and Jarrold, M. F., Rev. Sci. Instrum. 1997, 68, 1122.
44. Sugai, T., Inakuma, M., Hudgins, R., Dugourd, P. Fye, J. L., Jarrold, M. F. and Shinohara, H., J. Am. Chem. Soc. 2001, 123, 6427.
45. Kimura, T., Sugai, T., and Shinohara, H., Int. J. Mass Spectrom. 1999, 188, 225.
46. Klingeler, R., Bechthold, P. S., Neeb, M., and Eberhardt, W., J. Chem. Phys. 2000, 113, 1420.
47. Yamaguchi, Y. and Maruyama, S., Chem. Phys. Lett. 1998, 286, 336.
48. Maruyama, S. and Yamaguchi, Y., Chem. Phys. Lett. 1998, 286, 343.
49. Dugourd, Ph., Hudgins, R. R., Tenenbaum, J. M., Jarrold, M. F., Phys. Rev. Lett. 1998, 80, 4197.
50. Guo, T., Jin, C. and Smalley, R. E., J. Phys. Chem. 1991, 95, 4948.
51. Muhr, H. J., Nasper, R., Schnyder, B. and Kotz, R., Chem. Phys. Lett. 1996, 249, 399.
52. See Review: Reuther, U. and Hirsch, A., Carbon, 2000, 38, 1539.
53. Kimura, T., Sugai, T., and Shinohara, H., Chem. Phys. Lett. 1996, 256, 269.
54. Fye, J. L. and Jarrold, M. F., J. Phys. Chem. A 1997, 101, 1836.
55. Ray, C., Pellarin, M., Lerme, J. L., Vialle, J. L., Broyer, M., Blasse, X., Melion, P., Keghelian, P. and Perez, A., Phys. Rev. Lett. 1998, 80, 5365.
56. Branz, W., Billas, I. M. L., Malinowski, N., Tast, F., Heinebrodt, M. and Martin, T. P., J. Chem. Phys. 1998, 109, 3425.
57. Shinohara, H., Advances Metal Semiconductor Clusters 1998, 4, 205.
58. Wang, C.-R., Kai, T., Tomiyama, T., Yoshida, T., Kobayashi, Y., Nishibori, E., Takata, M., Sakata, M., Shinohara, H., Nature 2000, 408, 426.
59. Stevenson, S., Fowler, P. W., Heine, T., Duchamp, J. C., Rice, G., Glass, T., Harich, K., Hajdull, E., Biblell, R. and Dorn, H. C., Nature 2000, 408, 428.
60. Ogawa, T., Sugai, T., Shinohara, H., Proc. Electrochem. Soc. 1999.
61. Inoue, T., Kubozono, Y., Kashino, S., Takabayashi, Y., Fujitaka, K., Hida, M., Inoue, M., Kanbara, T., Emura, S. and Uruga, T., Chem. Phys. Lett. 2000, 316, 381.
62. Guo, T., Smalley, and R. E., Scuseria, G. E., J. Chem. Phys., 1993, 99, 352.
63. Guo, B. C., Wei, S., Purnell, J., Buzza, S. and Castleman, Jr, A. W., Science 1992, 256, 515.

64. Wei, S., Guo, B. C., Deng, H. T., Kerns, K., Purnell, J., Buzza, S. A., Castleman, Jr., A. W., J. Am. Chem. Soc. 1994, 116, 4475.
65. Wang, L.-S. and Li, X., J. Chem. Phys. 2000, 112, 3602.